Applied element method simulation of experimental failure modes in RC shear walls

Corneliu Cismasiu[1a], António Pinho Ramos[*1b], Ionut D. Moldovan[2c], Diogo F. Ferreira[1d] and Jorge B. Filho[3e]

[1]*CERIS, ICIST and Department of Civil Engineering, Faculdade de Ciências e Tecnologia,
Universidade NOVA de Lisboa, 2829-516 Caparica, Portugal*
[2]*CERIS, Instituto Superior Técnico, Universidade de Lisboa, 1049-001, Lisboa, Portugal*
[3]*Department of Structures, Universidade Estadual de Londrina, Paraná, Brazil*

Abstract. With the continuous evolution of the numerical methods and the availability of advanced constitutive models, it became a common practice to use complex physical and geometrical nonlinear numerical analyses to estimate the structural behavior of reinforced concrete elements. Such simulations may yield the complete time history of the structural behavior; from the first moment the load is applied until the total collapse of the structure. However, the evolution of the cracking pattern in geometrical discontinuous zones of reinforced concrete elements and the associated failure modes are relatively complex phenomena and their numerical simulation is considerably challenging. The objective of the present paper is to assess the applicability of the Applied Element Method in simulating the development of distinct failure modes in reinforced concrete walls subjected to monotonic loading obtained in experimental tests. A pushover test was simulated numerically on three distinct RC shear walls, all presenting an opening that guarantee a geometrical discontinuity zone and, consequently, a relatively complex cracking pattern. The presence of different reinforcement solutions in each wall enables the assessment of the reliability of the computational model for distinct failure modes. Comparison with available experimental tests allows concluding on the advantages and the limitations of the Applied Element Method when used to estimate the behavior of reinforced concrete elements subjected to monotonic loading.

Keywords: applied element method; nonlinear analysis; cracking pattern; RC shear walls

1. Introduction

Nowadays, due to the readily available computing facilities and highly accurate constitutive models, it is common practice to use complex physical and geometrical nonlinear numerical analyses to estimate the structural behavior of reinforced concrete elements. The associated numerical simulations may yield important data for a performance-based design, including the complete time history of the structural behavior, from the first moment the load is applied, until the total collapse of the structure. However, the evolution of the cracking pattern in geometrical discontinuous zones of RC elements and the associated failure modes are relatively complex and, despite the great effort that has been made to develop performing numerical models, e.g., Ngo and Scordelis (1967), Vecchio (1989), Vecchio and Collins (1993), Yang and Chen (2005), Azevedo *et al.* (2010), Dujc *et al.* (2010), Dominguez *et al.* (2010), Mamede *et al.* (2013), Croce and Formichi (2014), Balomenos *et al.* (2015), their simulation is still considerably challenging, ACI (1997), Maekawa and Okamura (2003), Borosnyói and Balázs (2005).

In 2001, Meguro and Tagel-Din presented a promising extension of the applied element method (Meguro and

Tagel-Din 2000), which can be used to perform nonlinear analysis of RC structures. With no need of any previous knowledge about the crack location or direction of propagation, complex phenomena such as crack initiation, propagation, opening and closure, could be simulated automatically, with reliable accuracy. The effectiveness of the method, as implemented in the nonlinear structural analysis software ELS (ASI 2013), to simulate different failure modes and cracking patterns in RC shear walls subjected to monotonic loading, is investigated in the present paper.

2. Applied element method

Although extremely important in performance-based design for safety and vulnerability assessment, the prediction of the structural response of RC structures when significant level of damage is expected is a considerably challenging problem. Numerical methods based on continuum material equations, like, for example, the finite element method, are known to perform poorly in the case of heavily damaged structures. In an attempt to improve the accuracy of the numerical simulations near collapse, an extension of the discrete element technique was proposed, Meguro and Hakuno (1989), Meguro and Tagel-Din (2000) and improved by Meguro and Tagel-Din (2001). In this technique, known as the Applied Element Method (AEM),

---

∗Corresponding author, Professor
 E-mail: ampr@fct.unl.pt

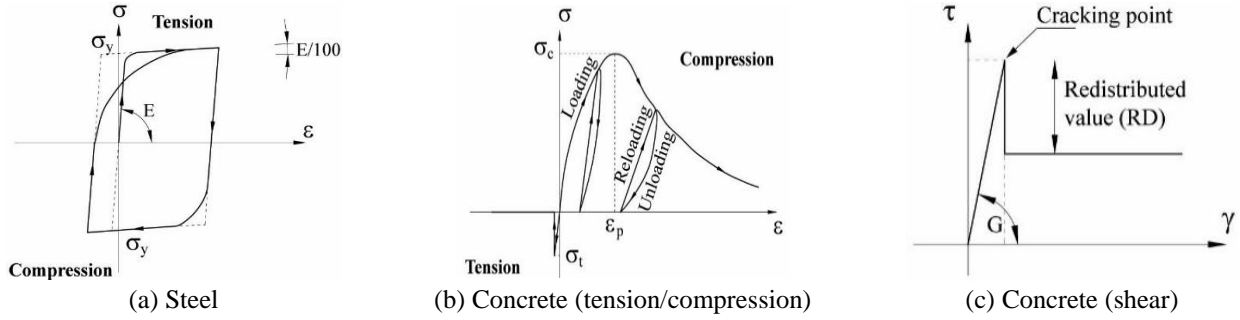(a) Steel (b) Concrete (tension/compression) (c) Concrete (shear)

Fig. 1 Constitutive models for steel and concrete in ELS

the structure is virtually divided into small rigid body elements, connected by pairs of normal and shear springs along the inter-element edges. The associated degrees of freedom are the rigid body displacements of each element, with the internal stresses and deformations concentrated at springs level. For this reason, although composed of an assembly of rigid bodies, the structure as a whole is deformable. Although the effect of the Poisson's ratio can be simulated using the AEM, Tagel-Din and Meguro (1998), Meguro and Tagel-Din (2000), it was disregarded when the method was implemented in the current version of the ELS. For this reason, the Poisson's ratio effect is not considered in the numerical simulations presented in the present paper.

In order to capture the nonlinear behavior of RC structures, the constitutive models presented in Fig. 1 are adopted in ELS for steel and concrete, respectively. The springs associated to rebars are modeled using the Ristic constitutive model (Ristic *et al*. 1986), as shown in Fig. 1(a). The tangent stiffness of the rebars is computed taking into account the current strain, loading status and previous loading history that controls the Bauschinger's effect. Fig. 1(b) illustrates the Maekawa constitutive model (Okamura and Maekawa 1991), which is associated to the normal springs representing concrete in compression or tension. The envelope of the stress-strain curve for compressed concrete is defined as a function of the initial Young's modulus, compressive plastic strain and a fracture parameter representing the extent of the initial damage in concrete. The tangent modulus is calculated based on the current strain and the loading phase. For concrete springs in tension, the spring stiffness is set to zero following cracking. The constitutive material model illustrated in Fig. 1(c) is associated to shear springs. Until cracking, stresses and strains are assumed to be proportional. After cracking, and to avoid numerical problems, a minimum value is assumed for the stiffness (1% of its initial value). The unbalanced stresses occurring during cracking are redistributed at each incremental step of the numerical analysis.

3. Experimental tests

The experimental specimens presented in this paper are rectangular RC shear walls with $1000\times1350\times120$ mm and a centered square opening 400 mm wide, located at the base
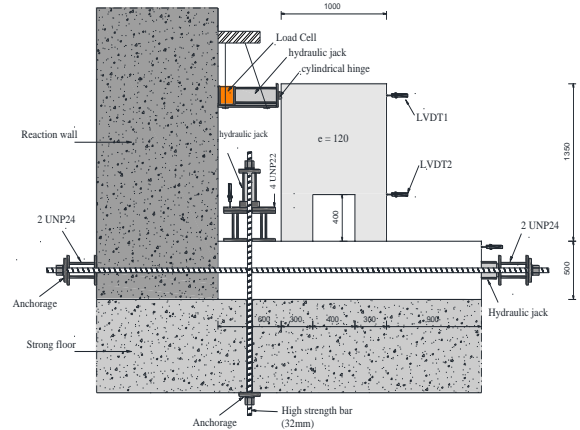

Fig. 2 Geometry of the specimen and test setup (dimensions in mm)

of the shear wall (see Fig. 2). The shear wall was clamped to a RC load-bearing beam of $2500\times800\times200$ mm. That beam was fixed to the laboratory strong floor using 4 high strength steel bars, which were prestressed with 350 kN/bar in the horizontal direction and 265 kN/bar in the vertical direction, in order to immobilize the specimens.

The horizontal loading was applied to the shear wall through a cylindrical steel hinge using a 900 kN capacity hydraulic jack. To measure the horizontal force, a load cell was used, positioned between the reaction wall and the hydraulic jack used to apply the horizontal force. Two LVDT were used to measure the horizontal displacements of the specimens. The displacements were measured at the top of the shear walls and at the upper part of the opening, on the opposite side to where the load was applied (Fig. 2). In the first load steps the horizontal load was applied in 20 kN increments, but after cracking it was reduced to 10 kN increments. A more detailed description of the experimental tests can be found in Bounassar (1995).

The shear wall specimens were designed using strut and tie models. Three different strut and tie models were used: model (a) where the horizontal load is mainly transferred by inclined compression ("compression model"-MB1); model (b) using a transversal tie ("tension model"-MB2); and model (c), using a combination of the two previous models ("mixed model"-MB3), see Fig. 3. A horizontal applied load (P_d) of 350 kN was considered in the design of all shear walls. The resulting reinforcement layouts are illustrated in Fig. 4.

(a) compression model   (b) tension model   (c) mixed model
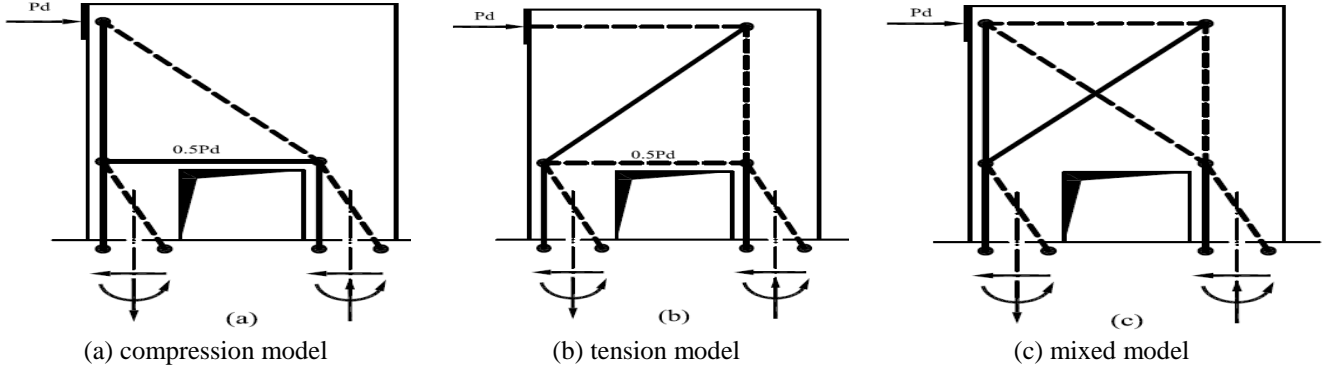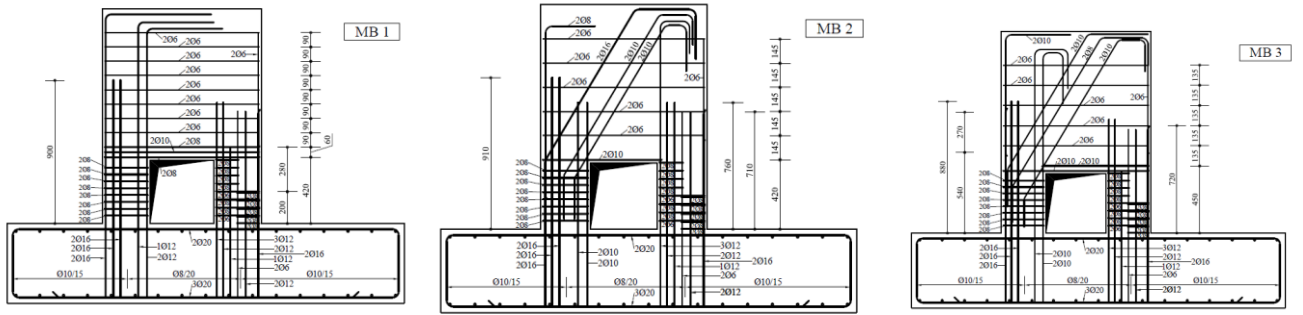
Fig. 3 Basic models of load transmission

Fig. 4 Reinforcement layouts (dimensions in mm)

Table 1 Mechanical characteristics of the concrete

Specimen	f_c (MPa)	f_{ck} (MPa)	f_{ct} (MPa)	E_c (GPa)
MB1, MB3	37.0	29.0	2.83	33.3
MB2	39.0	31.0	2.96	33.8

Table 2 Mechanical characteristics of the reinforcement bars

ϕ(mm)	6	8	10	12	16
f_y(MPa)	480	560	530	550	600
f_u(MPa)	630	644	670	616	666
e_u(%)	13.9	13.9	17.5	16.5	13.5

3.1 Material characterization

The concrete was made using locally available crushedcoarse limestone aggregate, along with medium and fine sand and Portland cement CEM II/B-L 32.5 N. The maximum aggregate size was 9.52 mm. The concrete compressive strength (f_c) was measured on 150×300 mm cylinders, according to EN 12390-3. The characteristic compressive strength (f_{ck}), the modulus of elasticity (E_c) and the tensile strength of the concrete (f_{ct}) were calculated from its compressive strength according to the fib Model Code 2010, Eqs. (1) to (3). The obtained results are listed in Table 1.

$$f_{ck} = f_c - 8 \quad [MPa] \tag{1}$$

$$E_c = 21.5\left(\frac{f_c}{10}\right)^{1/3} [GPa] \tag{2}$$

$$f_{ct} = 0.3(f_{ck})^{2/3}[MPa] \tag{3}$$

In order to determine the yield stress (f_y), the tensile strength (f_t) and the ultimate strain (e_u) of the longitudinal reinforcement, direct tensile tests were performed on coupons from the same steel batch, according to EN 10002-1. Those results are listed in Table 2.

A more detailed description of the experimental test campaign can be found in Bounassar (1995).

3.2 Analysis of the experimental results

The experimental capacity curves, expressing the relationship between the horizontal displacements recorded by transducers LVDT1 and LVDT2 (see Fig. 2) and the horizontal applied load, are illustrated in Fig. 5. The values of the cracking load (P_{cr}), corresponding to the load level for the first cracks visible to the naked eye, the ultimate load at failure (P_u) and the ratio between the experimental failure load and the design load (P_d) are collected in Table 3.

Analyzing Fig. 5, one can observe that, at the beginning of loading process, all three specimens exhibit similar stiffness. However, at failure, specimen MB2 presented higher horizontal deformations when compared to the others, due to a ductile failure through the transversal tie. Specimen MB1 presented a more brittle failure by the concrete crushing of the compression strut on the right-side short column. The premature failure of MB3 was caused by concrete crushing in the load application zone. Accordingly, it achieved a smaller ultimate load, presenting a slightly sub-unitary ratio between the experimental failure load and
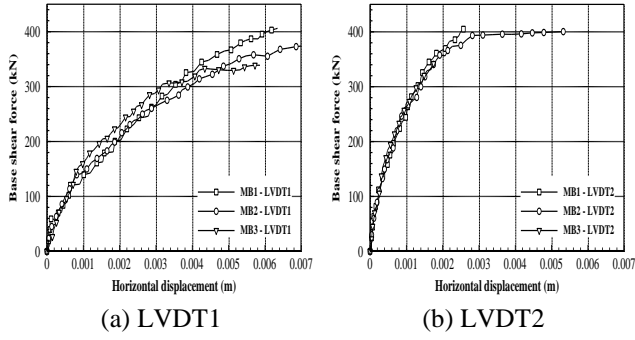
(a) LVDT1   (b) LVDT2

Fig. 5 Experimental capacity curves

Table 3 Experimental results

Specimen	P_d (kN)	P_{cr} (kN)	P_u (kN)	P_u/P_d
MB1	350	120	407	1.16
MB2	350	80	410	1.17
MB3	350	120	330	0.94

the design load. As illustrated in Table 3, in the other two specimens the obtained failure load was above the design load, with similar P_u/P_d ratios.

The beginning of cracking occurred for about the same load level in all the tested specimens, usually in the connection region between the left-side short column and the upper part of the shear wall. Nevertheless, specimen MB2 presented higher crack openings, especially in a region located on the left upper side of the shear wall, where tension stresses are present and the shear wall has a smaller amount of reinforcement.

4. Numerical modelling

To assess the reliability of the AEM in simulating the development of distinct failure modes in reinforced concrete walls subjected to monotonic loading, the experimental tests performed on the three shear walls described in Section 3 were simulated in ELS. The experimental pushover curves registered for each shear wall by the two LVDT presented in Fig. 2 are compared with the corresponding numerical estimates. Special attention is also paid to the direct comparison of the cracking patterns obtained in the laboratory and predicted by the numerical model.

The 3D geometry of the RC walls was accurately defined, taking into account the precise arrangement of the structural rebars. To guarantee a numerically converged solution, a sensitivity analysis was also performed, analysing the influence of the number of load steps, number of connecting springs between the elements, and the element size. Similar to the experimental procedure, the numerical analysis starts by characterizing the materials in the RC walls, namely the concrete and the steel in the rebars. The previously presented mechanical properties for concrete and steel, see Tables 1 and 2, were used to calibrate the relevant parameters defining the corresponding constitutive models.
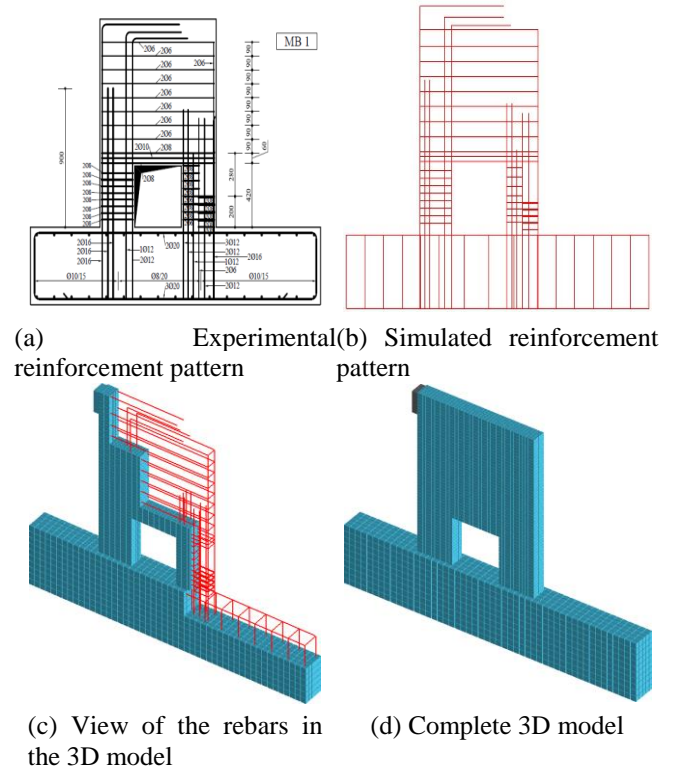

(a) Experimental reinforcement pattern   (b) Simulated reinforcement pattern

(c) View of the rebars in the 3D model   (d) Complete 3D model

Fig. 6 Three-dimensional model of MB1 shear wall

4.1 Spatial geometry modeling of the RC walls

The three structures under analysis in the present paper have the same external geometry, composed by a rectangular shear wall, clamped to a load-bearing beam and with a square opening located at the base of the wall. Each structure has a distinct reinforcement pattern, designed to ensure distinct failure mechanisms, as described above. The reinforcement steel bars are inserted in the 3D numerical model taking into account their cross-section and layout, as illustrated in Fig. 6 for one of the shear walls.

4.2 Sensitivity analysis

In order to guarantee the convergence of the numerical solution, a mesh sensitivity analysis was performed, studying the effect of the element size and the number of connecting springs between elements.

It is known (Meguro and Tagel-Din 2000), that AEM numerical simulations performed with large-size elements yield over-stiff solutions, meaning that the simulated failure loads result larger than the real solution. On the other hand, the number of connecting springs between elements is an important factor as well. While this number does not affect the stiffness of the elements associated to translational degrees of freedom, it directly affects the rotational stiffness. However, this error becomes insignificant for small-sized elements, as the relative rotation between adjacent elements becomes small. Exhaustive tests published in the literature (Meguro and Tagel-Din 2001), permitted to conclude that the use of a relatively large number of small-sized elements together with relatively

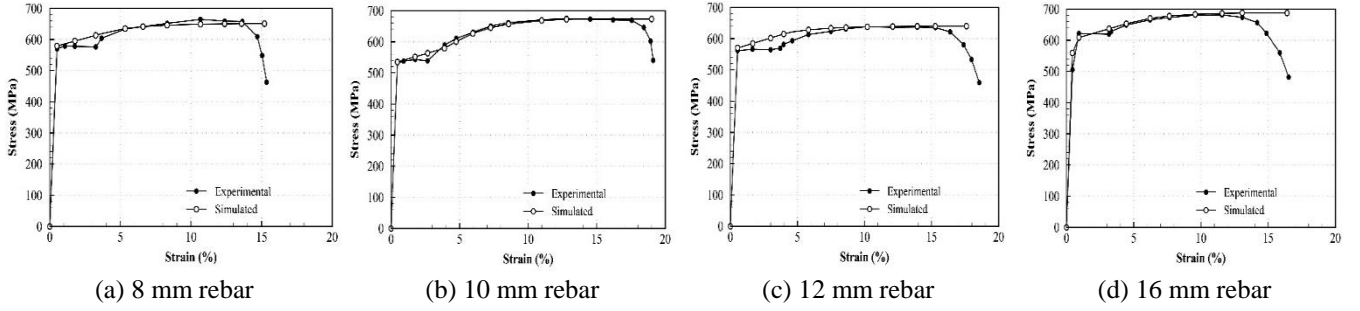| (a) 8 mm rebar | (b) 10 mm rebar | (c) 12 mm rebar | (d) 16 mm rebar |

Fig. 7 Comparison between the experimental and simulated steel tensile tests
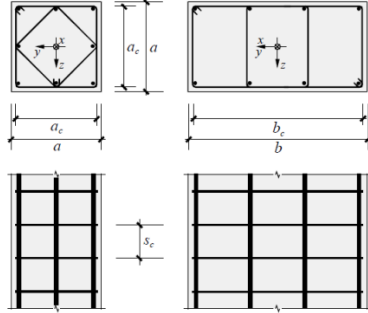
Fig. 8 Compressive rectangular cross-section members with confining reinforcement

Table 4 Mechanical characteristics of the concrete used in the numerical modelling

Specimen	Confinement	f_c(MPa)	f_{ck}(MPa)	f_{ct}(MPa)	E_c(GPa)
MB1, MB3	Zone 1	47.2	39.2	3.46	36.1
	Zone 2	50.9	42.9	3.68	37.0
MB2	Zone 1	50.0	42.0	3.62	36.8
	Zone 2	53.9	45.9	3.85	37.7
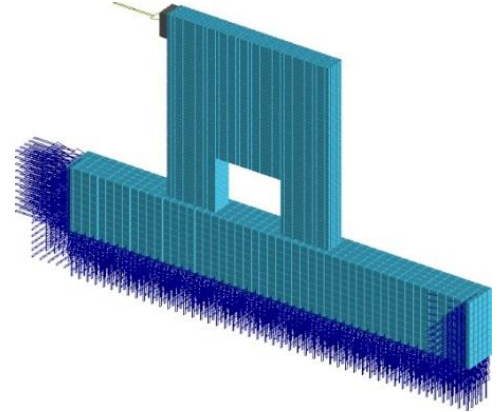
Fig. 9 Numerical model MB1: Boundary conditions and applied load

small number of connecting springs leads to highly accurate solutions in reasonable CPU time.

To study the convergence of the AEM solution, the shear wall MB1 was analyzed using three increasingly smaller-sized elements (approximately cubic shapes with edges of 50, 25 and 16.7 mm). Additionally, for each different element size, two models were considered, using 5 and 10 connecting springs for each pairs of adjacent element faces. The convergence was considered achieved when the changes in the capacity curves from one analysis to the next were too small to be visually noticeable. The estimates for the capacity curve stabilized for a mesh consisting of 35120 elements (edge of 25 mm) and 5 connecting springs between element faces and therefore, this combination was considered an appropriate mesh and used for all the tests reported in this paper.

A similar analysis was performed to calibrate the loading increment on model MB1. Pushover curves were obtained using 700 and 1000 loading increments and no noticeable differences were obtained between the resulting capacity curves. The loading increment was thus defined as 1.0 mm per step for all models.

4.3 Calibration of the constitutive models

4.3.1 Steel

The steel stress-strain curves obtained experimentally for the material characterization under tensile tests were simulated numerically and used to calibrate the parameters defining the Ristic constitutive model of steel (Ristic *et al*. 1986). The mechanical properties presented in Table 2 were used, considering a Young's Modulus of 200 GPa, a shear modulus of 79.9 GPa and a post yield stiffness factor of 0.01. A comparison between the experimental and simulated

stress-strain curves for all rebars used in the reinforcement of the shear walls is illustrated in Fig. 7.

4.3.2 Concrete

The addition of stirrups is known to provide confinement and to increase the ultimate compressive strength of the concrete (fib Model Code 2010). To take into account this effect in the numerical model, two levels of confinement were considered, namely a relatively loose confinement in the upper part of the shear wall and the load-bearing beam (Zone 1) and a stronger confinement justified by the dense stirrup distribution in the area of the short columns (Zone 2). According to fib Model Code 2010, the compressive strength of the confined concrete, f_{ckc}, can be computed using Eq. (4).

$$\frac{f_{ck,c}}{f_{ck}} = 1 + 3.5\left(\frac{\sigma_2}{f_{ck}}\right)^{3/4} \qquad (4)$$

The confining pressure σ_2 can be calculated, for rectangular cross-sections, using Eq. (5) with ω_c defined by Eq. (6).
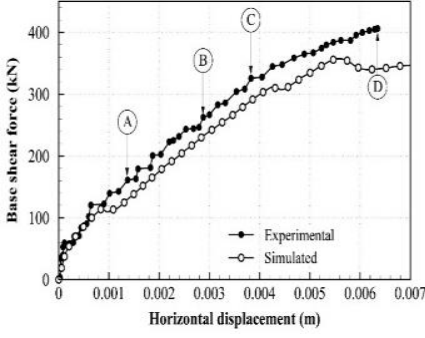
Fig. 10 Experimental and simulated capacity curves for the MB1 model at LVDT1
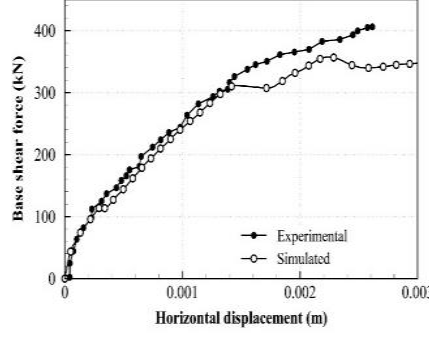

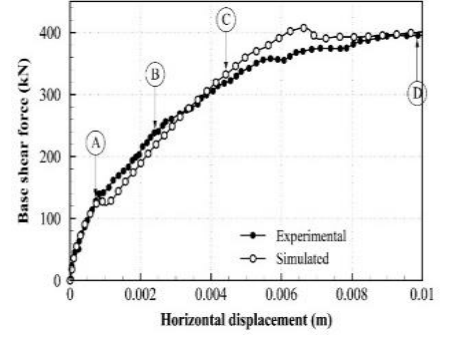Fig. 11 Experimental and simulated capacity curves for the MB1 model at LVDT2

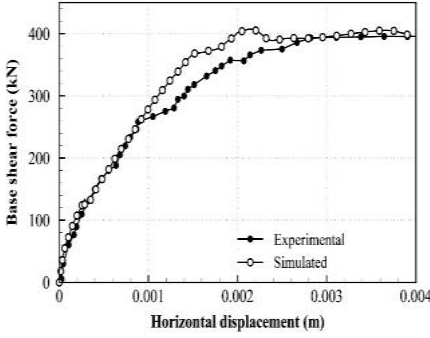Fig. 12 Experimental and simulated capacity curves for the MB2 model at LVDT1

Fig. 13 Experimental and simulated capacity curves for the MB2 model at LVDT2
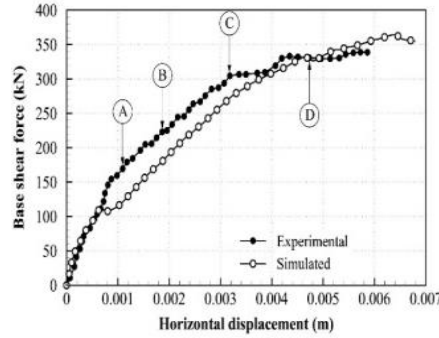

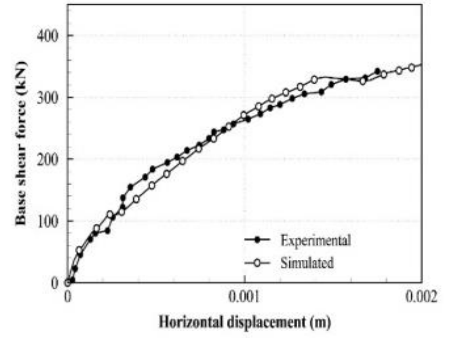Fig. 14 Experimental and simulated capacity curves for the MB3 model at LVDT1

Fig. 15 Experimental and simulated capacity curves for the MB3 model at LVDT2

$$\sigma_2 = \omega_c f_{cd} \left(1 - \frac{s_c}{a_c}\right)\left(1 - \frac{s_c}{b_c}\right)\left(1 - \frac{\sum_i b_i^2/6}{a_c b_c}\right) \qquad (5)$$

$$\omega_c = \min\left\{\omega_y = \frac{A_{sy} f_{yd}}{a_c s_c f_{cd}}, \omega_z = \frac{A_{sz} f_{yd}}{b_c s_c f_{cd}}\right\} \qquad (6)$$

In Eqs. (5) and (6), f_{cd} is the design value of cylinder compressive strength of concrete, f_{yd} is the design yield strength of reinforcing steel, A_{sy} and A_{sz} are the areas of reinforcement in the y and z direction, respectively, b_i is the center line spacing along the section parameter of longitudinal bars (indexed by i) engaged by a stirrups corner or a cross-tie, and a_c, b_c and s_c are representative distances defined in Fig. 8.

The resulting mechanical characteristics adopted for the confined reinforced concrete in the numerical simulation of the three tested shear walls are listed in Table 4.

The average values for the mechanical properties of the concrete presented in Table 4 were used to calculate the parameters defining the Maekawa constitutive model (Okamura and Maekawa 1991) used for concrete. The concrete shear modulus was taken as $E/2(1+v)$ and a Poisson ratio (v) of 0.2 was considered.

Another important parameter characterizing the material constitutive models in ELS is the separation strain. This parameter defines the strain value in the springs located between two neighboring elements at which the elements

Table 5 Relative errors of the numerical solutions

Relative error (%)	LVDT1	LVDT2
MB1	11.2	9.0
MB2	5.3	6.1
MB3	9.3	6.0

are considered to be physically separated. According to the ELS Modeling Manual (ASI 2010), for reinforced concrete elements, the separation strain should be higher than the ultimate tensile strain of the rebars. Taking into account the tensile strains presented in Fig. 7 and Table 2, the separation strain was set to 0.2 for all the numerical models presented in the present paper.

4.4 Boundary conditions

The results obtained from a nonlinear analysis using solid elements are highly sensitive to the accurate definition of the boundary conditions. To simulate the experimental boundary conditions, the load-bearing beam was considered clamped on the two ends and the bottom surfaces, as illustrated in Fig. 9. To avoid stress singularity and in accordance with the experimental procedure, the applied load is transmitted to the structure through a 200×120×5 mm metallic plate.

Taking into account that a significant reduction in the structural stiffness is expected in the numerical simulations of the pushover tests due to severe cracking and crushing of the concrete and eventual failure of the reinforcement steel, a displacement loading control is used to obtain the capacity
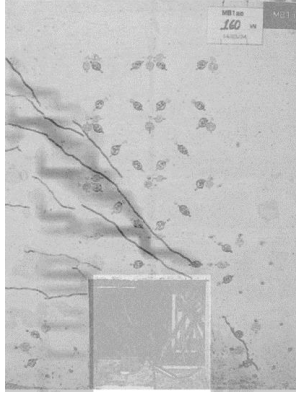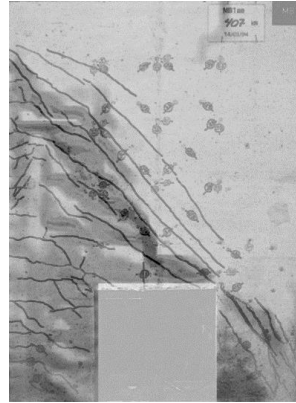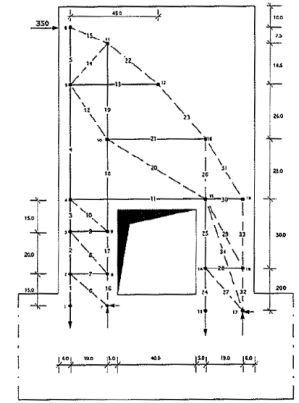
(a) Point A: V_{exp}=160 kN, V_{num}=130 kN
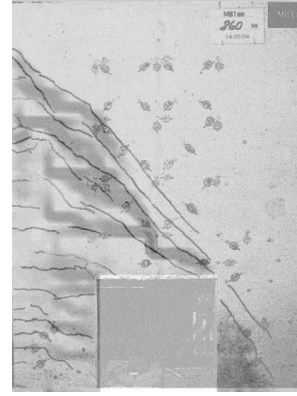
(b) Point B: V_{exp}=260 kN, V_{num}=230 kN
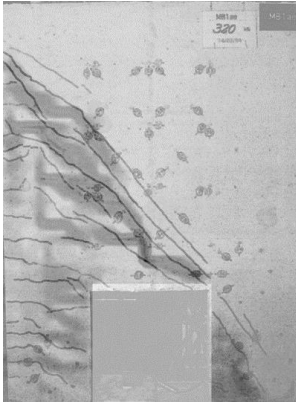
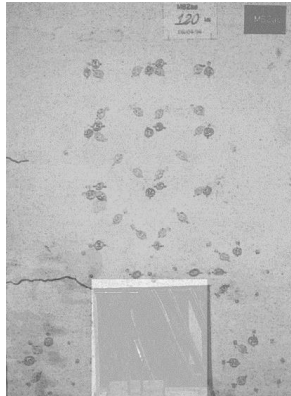(c) Point C: V_{exp}=320 KN, V_{num}=287 kN

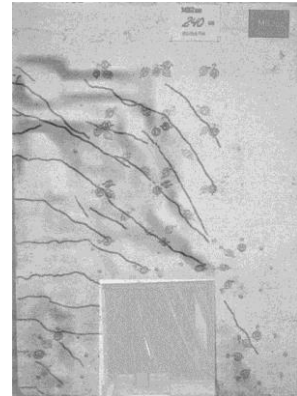(d) Point D: V_{exp}=407 KN, V_{num}=340 kN
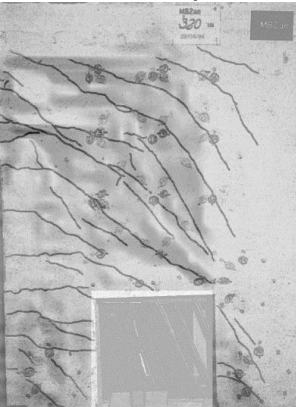

(e) Strut and tie model

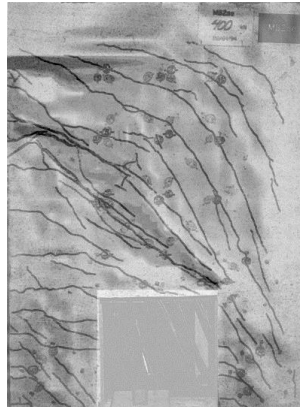Fig. 16 Model MB1-cracking pattern at selected points and collapse mechanism

(a) Point A: V_{exp}=120 KN, V_{num}=120 kN
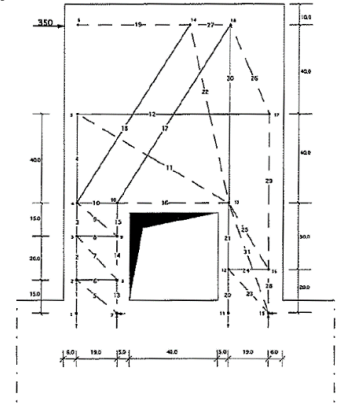

(b) Point B: V_{exp}=240 KN, V_{num}=220 kN

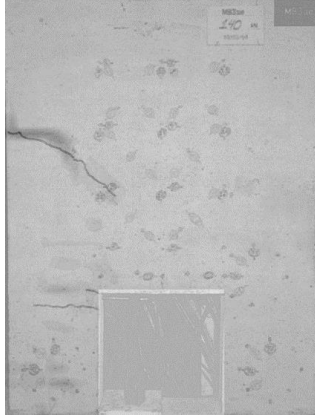(c) Point C: V_{exp}=320 KN, V_{num}=335 kN
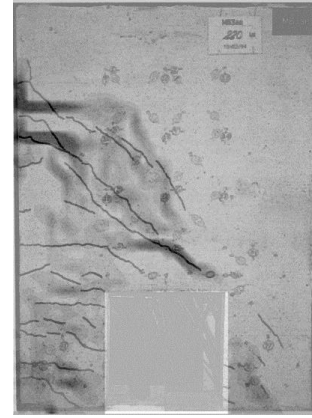

(d) Point D: V_{exp}=400 KN, V_{num}=400 kN
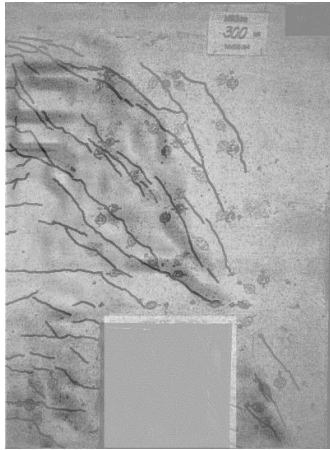

(e) Strut and tie model

Fig. 17 Model MB2-cracking pattern at selected points and collapse mechanism
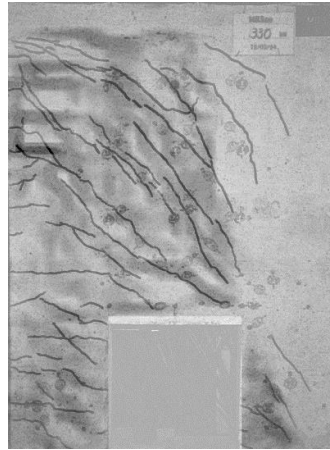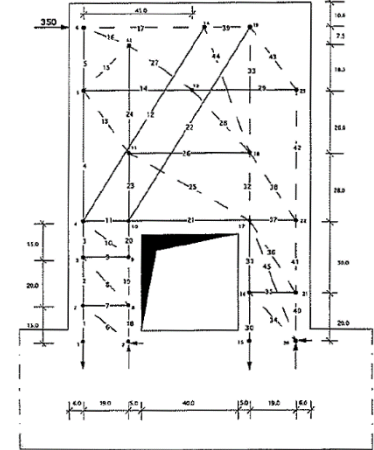
(a) Point A: V_{exp}=140 KN, V_{num}=110 kN

(b) Point B: V_{exp}=220 KN, V_{num}=175 kN

(c) Point C: V_{exp}=300 KN, V_{num}=270 kN

(d) Point D: V_{exp}=330 KN, V_{num}=330 kN

(e) Strut and tie model

Fig. 18 Model MB3-cracking pattern at selected points and collapse mechanism

curves. The displacements were applied in 1.0 mm steps.

4.5 Comparison between the simulated and experimental results

The experimental and numerical results obtained for the three reinforcement setups and testing sequences presented in Section 3 are compared in this section. The comparison endorses a thorough assessment of the reliability of the applied element-based computational model in recovering the experimental capacity curves and in simulating the distinct failure modes and cracking patterns.

4.5.1 Capacity curves
Similar to the experimental test, the simulated capacity curves are obtained by plotting the total base shear force against the horizontal displacements measured in the vicinity of the two displacement transducers (LVDT1 and LVDT2) presented in Fig. 2. Two capacity curves are thus obtained for each model, one for each LVDT. The experimental capacity curves are plotted in Figs. 10 to 15 (dark markers) against their simulated counterparts (light markers).

The overall agreement between the experimental and numerical results is rather good, except the capacity curve of the MB1 model recorded at the LVDT1 transducer. The numerical model recovers well the global stiffness deterioration of the shear walls until roughly 80% of their bearing capacity, as visible by comparing the slopes of the experimental and simulated capacity curves along the A-B-C paths identified on the LVDT1 plots. The differences between the base shear values along these paths may, however, be considerable, as visible in Fig. 10 and, especially, Fig. 14. These differences are justified by the occurrence of a rapidly propagating crack in the numerical model (softening in tension is not considered in the Maekawa concrete constitutive model, see Fig. 1(b)), which leads to sudden strain localization, thus releasing some of the base shear. This effect, visible in the 'bumps' occurring around 120-140 kN of base shear in all simulated capacity curves, was not observed in the force-driven experimental tests. However, the stiffness reduction corresponding to this event seems to take place in the experimental model as well, leading to the similar stiffness predictions on the A-B-C loading paths. The simulated cracking pattern causing this stiffness degradation is also in good accordance with the experimental results, as shown in the next section, although it seems that the numerical model over-estimates the suddenness of the cracking event and the subsequent strain localization. A second, and less dramatic, propagating cracking event is recorded by the numerical models MB1 and MB2 around 300 kN and 400 kN of base shear, respectively (see Figs. 10 to 13), but once again its occurrence seems not to have such noticeable effect in the experimental results (although slightly visible in Fig. 10).

In order to quantify the quality of the AEM solutions and to endorse a direct comparison between different models, the relative error of the numerical solution is defined as the area comprised between the experimental and simulated capacity curves in Figs. 10 to 15, normalized to the total area under the experimental capacity curve,

$$\varepsilon = \frac{\int_0^{u_{max}} |V_{exp} - V_{num}| \, du}{\int_0^{u_{max}} V_{exp} \, du} \quad (7)$$

In Eq. (7), V_{exp} and V_{num} are the values of the base shear in the experimental and simulated capacity curves, respectively, and u_{max} is the maximum horizontal displacement recorded experimentally. The relative errors for each of the six plots are presented in Table 5.

With the exception of the capacity curve of the MB1 model read at LVDT1, the relative errors of the AEM solution are situated between 5 and 10%, which is considered sufficient for practical purposes.

4.5.2 Cracking patterns

A readily interpretable representation of the simulated cracks' size and localization is the plot of the principal strain contours. Using the element size, the strains can be directly connected to the crack opening, facilitating the comparison with the experimental results. During the experimental campaign the cracking patterns developed in the tested RC walls were recorded for different load levels (Bounassar 1995). These images were used to assess the ability of the AEM to accurately simulate the developing of the cracking patterns in RC shear walls. To illustrate this ability, the experimental and simulated cracking patterns corresponding to the points A to D showed in Figs. 10, 12 and 14 are overlaid and presented in Figs. 16 to 18 for the MB1, MB2 and MB3 models, respectively. After the cracking plots corresponding to points D in Figs. 10, 12 and 14 (i.e., near the ultimate load), the collapse mechanism assumed for the reinforcement design is also presented for illustrative purposes. It is noted that the simulated cracking patterns correspond to the same abscissa as indicated by points A to D, meaning that the base shear forces may be different on the experimental and simulated plots (but the lateral displacements are the same). In all plots, darker areas indicate more pronounced cracks.

The AEM implemented in ELS uses a discrete crack approach, meaning that cracks can only develop at the surface of the elements. For this reason, and to improve the accuracy, the adopted element size must be smaller than the expected crack spacing. As the element size was 25 mm in all analyses reported here, one cannot expect to reproduce smaller crack spacing. Nevertheless, the cracking pattern observed experimentally is consistently reproduced by the AEM model at all tested loading points and for all models under analysis. The sequence of emergence and propagation of the cracks is also consistently reproduced by the simulations. The collapse mechanisms assumed in the design of the shear walls correspond to those observed experimentally and predicted by the numerical model.

5. Conclusions

In this paper, the experimental tests carried out on three RC shear walls containing a centered square opening are presented, together with the corresponding numerical simulation performed using the Applied Element Method. Regarding the experimental results, one may observe that the "tension model" shear wall (MB2) presented the higher horizontal deformations, due to a more ductile failure mobilized through the transversal tie. This model also presented the larger crack openings, especially on the left upper side of the shear wall, that had only a small amount of tensile reinforcement. The "compression model" (MB1) achieved a similar failure load for a less ductile failure mechanism. The premature failure load of model MB3 was caused by concrete crushing in the load application zone.

In what concern the numerical simulation, one can conclude that the AEM was able to predict with good accuracy the load-deformation curve, the failure loads and modes as well as the cracking patterns.

References

ACI Report 446.3R-97 (1997), *Finite Element Analysis of Fracture in Concrete Structures: State-of-the-Art*.

ASI (2010), *Extreme Loading for Structures V3.1 Modeling Manual*, Applied Science International, Durham, NC, U.K.

ASI (2013), *Extreme Loading for Structures Theoretical Manual*, Applied Science International, Durham, NC, U.K.

Azevedo, N.M., Lemos, J.V. and Almeida, J.R. (2010), "A discrete particle model for reinforced concrete fracture analysis", *Struct. Eng. Mech.*, **36**(3), 343-361.

Balomenos, G.P., Genikomsou, A.S., Polak, M.A. and Pandey, M.D. (2015), "Efficient method for probabilistic finite element analysis with application to reinforced concrete slabs", *Eng. Struct.*, **103**(15), 85-101.

Borosnyói, A. and Balázs, G.L. (2005), "Models for flexural cracking in concrete: The state of the art", *Struct. Concrete*, **6**(2), 53-62.

Bounassar Filho, J. (1995), "Dimensionamento e comportamento do betão estrutural em zonas com descontinuidades", Ph.D. Dissertation, Instituto Superior Técnico, Lisboa, Portugal.

Croce, P. and Formichi, P. (2014), "Numerical simulation of the behaviour of cracked reinforced concrete members", *Mater. Sci. Appl.*, **5**, 883-894.

Dominguez, N., Fernandez, M.A. and Ibrahimbegovic, A. (2010), "Enhanced solid element for modelling of reinforced-concrete structures with bond slip", *Comput. Concrete*, **7**(4), 347-364.

Dujc, J., Brank, B., Ibrahimbegovic, A. and Brancherie, D. (2010), "An embedded crack model for failure analysis of concrete solids", *Comput. Concrete*, **7**(4), 331-346.

EN 10002-1 (2001), *Tensile Testing of Metallic Materials Method of Test at Ambient Temperature*.

EN 12390-3 (2009), *Testing Hardened Concrete Compressive Strength of Test Specimens*.

Maekawa, K., Okamura, H. and Pimanmas, A. (2003), "Non-linear mechanics of reinforced concrete", CRC Press.

Mamede, N.F., Pinho Ramos, A. and Faria Duarte, M.V. (2013), "Experimental and parametric 3D nonlinear finite element analysis on punching of flat slabs with orthogonal reinforcement", *Eng. Struct.*, **48**, 442-457.

MC2010 (2013), *Fib Model Code for Concrete Structures*, Ernst & Sohn.

Meguro, K. and Hakuno, M. (1989), "Fracture analyses of concrete structures by the modified distinct element method", *Struct. Eng./Earthq. Eng.*, **6**(2), 283-294.

Meguro, K. and Tagel-Din, H. (2000), "Applied element method for structural analysis: theory and application for linear materials", *Struct. Eng. Earthq. Eng.*, **17**(1), 21-35.

Meguro, K. and Tagel-Din, H. (2001), "Applied element simulation of RC structures under cyclic loading", *J. Struct. Eng.*, **127**(11), 1295-1305.

Ngo, D. and Scordelis, A.C. (1967), "Finite element analysis of reinforced concrete beams", *ACI J.*, **64**(3), 152-163.

Okamura, H. and Maekawa, K. (1991), *Nonlinear Analysis and Constitutive Models of Reinforced Concrete*, Gihodo-Shuppan Co., Tokyo, Japan.

Ristic, D., Yamada, Y. and Iemura, H. (1986), "Stress-strain based modeling of hysteretic structures under earthquake induced bending and varying axial loads", Kyoto University, Japan.

Tagel-Din, H. and Meguro, K. (1998), "Consideration of Poisson's ratio effect in structural analysis using elements with three degrees of freedom", *Bull. Earthq. Resist. Struct. Rese. Center*, Institute of Industrial Science, The University of Tokyo, Japan.

Vecchio, F.J. (1989), "Nonlinear finite element analysis of reinforced concrete membranes", *ACI Struct. J.*, **86**(1), 26-35.

Vecchio, F.J. and Collins, M.P. (1993), "Compression response of cracked reinforced concrete", *J. Struct. Eng.*, **119**(12), 3590-3610.

Yang, Z.J. and Chen, J. (2005), "Finite element modeling of multiple cohesive discrete crack propagation in reinforced concrete beams", *Eng. Fract. Mech.*, **72**(14), 2280-2297.

CC